Pure & Appl. Chem., Vol. 68, No. 5, pp. 1107–1112, 1996.
Printed in Great Britain.

Analysis of Coulomb-crystal formation process for application to tailored particle synthesis in RF plasmas

Kunihide TACHIBANA and Yasuaki HAYASHI*

Department of Electronic Science and Engineering, Kyoto University,
Yoshida-honmachi, Sakyo, Kyoto 606 Japan
*Department of Electronics and Information Science, Kyoto Institute of Technology,
Matsugasaki, Sakyo, Kyoto 606, Japan

Abstract - By using newly developed Mie-scattering ellipsometry (MSE), the growth of carbon particles injected in a methane rf plasma was monitored. It was observed even by unaided eyes that the particles became arranged in hexagonal lattice structure. The particles were identified by a scanning electron microscope observation to have monodisperse spherical shapes grown to μm size by uniform coating . This Coulomb-solidification process was analyzed by MSE with the aid of video and photographic monitoring. The Coulomb-coupling parameter at the liquid-to-solid phase transition was estimated to be around 200, which is close to a theoretically predicted value of 170. Conditions of faster and efficient growth were also investigated for application to tailored particle synthesis.

INTRODUCTION

Recently dusty plasmas have been investigated intensively(1), and much effort is being paid for getting rid of particles in microelectronics manufacturing(1). On the other hand, dusty plasmas which contain a substantial number of negatively charged particles show interesting characteristics which differ from those of ordinary plasmas. One noticeable feature is the formation of Coulomb solids, as predicted by a theoretical consideration of Ikezi(2). Triggered by this prediction, three successful results were independently published last year, almost at the same time(3-5). Coulomb solidification is also of interest in the fields such as space plasma physics and solid state physics because a laboratory Coulomb crystal can be a visual model in microscopic or macroscopic scale for the problems in those fields. From a technological viewpoint, the process may be used for the synthesis of particles with tailored structures because the solidification can provide a method for mass manipulation of particles without mutual coagulation. However, it is important for such purpose to have a suitable method for *in situ* monitoring of particle behaviors and properties, and to understand the mechanisms involved in the solidification process in more detail.

Recently we have developed a Mie-scattering ellipsometry (MSE) method(6) and monitored the growth of carbon particles injected in a methane plasma(7). In our experiment a Coulomb solid has been successfully formed from particles grown to μm size(3). Discontinuous changes were observed in both the growth rate and the density decrease at about 30 min after the particle injection. This period of time matches well with the transition from liquid to solid phases as verified by side and top viewed photographs. In this paper, we review briefly the MSE method and then describe the results of particle growth and Coulomb-solidification processes with the aid of observations by a video camera and a scanning electron microscope (SEM). From the obtained results on the shape, size, distribution , density, and charge of particles, the Coulomb-coupling parameter is estimated and discussed for the solidification condition. In the last part, some experiments for the faster and efficient growth of spherical carbon particles are tried by changing the plasma conditions and the feed gases.

MIE-SCATTERING ELLIPSOMETRY

For spherical monodisperse particles, the ellipsometric parameters (Ψ, Δ) for the Mie scattered light are defined by the ratio of the scattering amplitude function of a parallel polarization component in the scattering plane S_2 to that of a perpendicular one S_1 as follows(6); $\tan\Psi \exp(i\Delta) = S_2/S_1$, where S_1 and S_2 are functions of the scattering angle, the diameter of particles, and the refractive index(8). When particles have polydisperse size distribution, the scattered light generally results in some depolarization

even if the incident light is fully polarized. In this case the Stokes vector (I, Q, U, V) is used for the calculation of the polarization state(6,9). The resultant Stokes vector for polydisperse particles is obtained by the summation of each component over the size distribution as $X = \Sigma X_i$ (X = I, Q, U, V). Then the ellipsometric parameters (Ψ, Δ) can be obtained from the following relations; $Q/I = -\cos(2\Psi)$, $U/I = \mu \sin(2\Psi)\cos(\Delta)$, $V/I = -\mu \sin(2\Psi)\sin(\Delta)$, where μ is the degree of coherence which appears due to the imperfect coherency of the two polarization components for polydisperse particles. Therefore, the ellipsometric parameters can be obtained independently of μ from the four components of the Stokes vector as functions of mean size and size distribution.

The arrangement for the Mie-scattering ellipsometry is shown in Fig.1(a). The light beam from an argon-ion laser (wavelength: 488 nm, output power: 100 mW) was linearly polarized at a 45° azimuth from the plane of scattering by a Glan-Taylor prism polarizer. After the scattering from particles in the plasma, the polarization state of the scattered light was measured at a right angle from the incident beam by use of a rotating-analyzer system(10). The sets of components (I, Q, U) and (I, Q, V) were obtained without and with placing a quarter-wave plate, respectively, of which the fast axis was set at an azimuth of 90° .

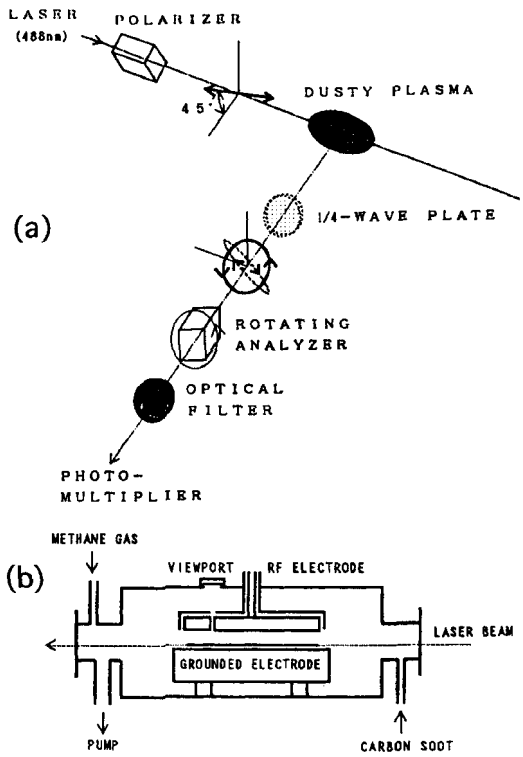

Fig.1 Schemes of (a) arrangement for Mie-scattering ellipsometry and (b) experimental chamber for the carbon particle growth.

GROWTH OF CARBON PARTICLES

A parallel-plate rf (13.56MHz) discharge reactor equipped with a rectangular rf electrode of 18 cm x 5 cm and a grounded electrode of 22 cm x 6.5 cm at a separation of 2.5 cm was used in the experiment as shown in Fig.1(b). Pure methane gas was introduced into the chamber at a position far from the plasma region in order not to disturb the trapped particles with its flow. After the initiation of discharge at a pressure of 40 Pa, a flow rate of 16 cm^3/min and an rf power of 10 W, the fine particles of carbon soots were supplied at one burst with a some amount of methane into the plasma. After the injection of carbon soots in the plasma, the bright region of Mie scattering within an expanded laser beam were observed visually. The region existed near the sheath-plasma boundary below the rf electrode in the early period. As the particles grow, they move by gravity toward the the plasma-sheath boundary over the grounded electrode and finally remain there, suspended by a balance of various forces acting on them The ellipsometric measurement was performed with a collimated laser beam of 1.4 mm diameter at a fixed vertical position 0.6 cm above the grounded electrode on the center axis, which was located near the plasma-sheath boundary. The evolution of the ellipsometric parameters from 3 min to 30 min is shown

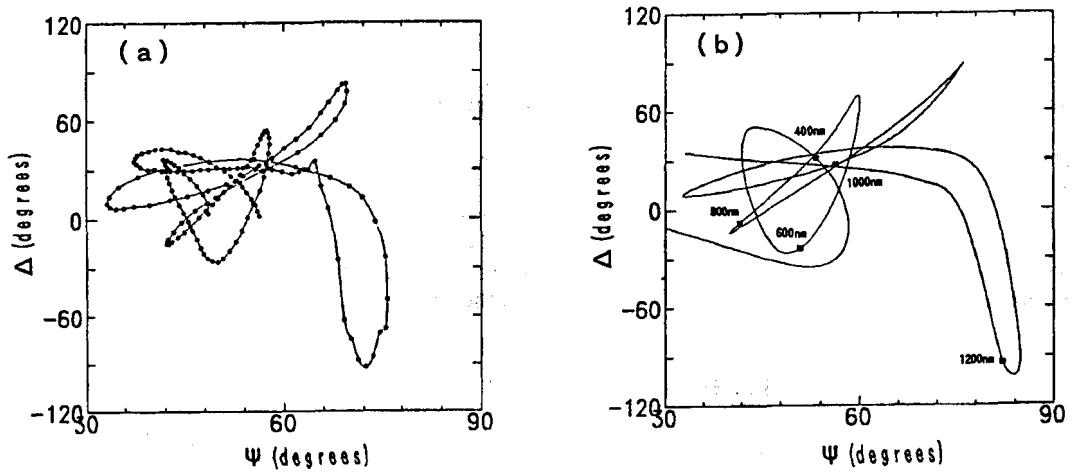

Fig.2 The (Ψ, Δ) trajectories obtained by (a) experiment and (b) simulation for the growing particles (experimental points are plotted every 10 s).

on the Ψ-Δ coordinate plane in Fig.2(a). First , the parameter Ψ increased gradually with a slight change of Δ, and at $\Psi > 45^{\circ}$, drawing counterclockwise loops on the coordinate plane.

The simulation of ellipsometric parameters was performed assuming spherical shapes with a variable complex reflective index $n = n_1 + i\, n_2$(6). As for the size distribution, the log-normal distribution function was assumed as

$$N(d) = \frac{1}{(2\pi)^{1/2}\ln(\sigma)d}\exp\left[-\frac{\{\ln(d) - \ln(d_m)\}^2}{2\{\ln(\sigma)\}^2}\right], \qquad (1)$$

where d is the particle diameter, d_m the geometric mean diameter, and σ the geometric standard deviation. As the particle diameter was increased, the trajectory turned clockwise for absorbing particles ($n_2 \neq 0$) ,while it did counterclockwise for non-absorbing particles ($n_2 = 0$). From the comparison of experimental results with the calculation, it is seen that the growing particles are non-absorbing at 488 nm. As for σ, the calculated trajectory converged to certain values with larger σ values. From the experimental trajectory it is suggested that the standard deviation must decrease as the particle diameter increases. This means that the size distribution of the particles has changed from polydisperse to rather monodisperse. Thus, a modified size distribution function was assumed, which was the log-normal for the first injected carbon particles and the translation-operated log-normal on a linear size scale for the grown particles. Figure 2 (b) shows the result of the simulation, in which the geometric mean size of 50 nm, the geometric standard deviation of 1.5 are taken for the distribution of the initially injected particles and the refractive index of the growing particles is taken to be 1.53. The simulated trajectory agrees with the experimental results. The deviation of the trajectory from the experimental one at the start (not shown in Fig.2) is attributed to the difference of the refractive index between pure carbon and hydrogenated carbon(7).

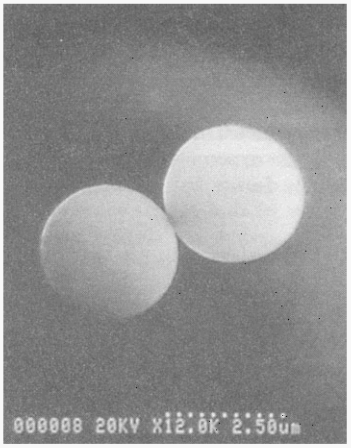

Fig.3 Typical SEM photograph of particles trapped in methane plasma for 180 min.

From the results the following scheme can be imagined for the growth of the carbon particles. The carbon soots were coated by hydrogenated amorphous carbon during the entrapment in a methane plasma. The smaller value of refractive index than that of a hydrogenated amorphous carbon film may be due to the lower density of the coated layer, in which the volume fraction of void is estimated to be 25%. The closer agreement of the trajectory by the model of translation-operated log-normal size distribution on a linear scale than that of log-normal with a constant geometric standard deviation indicates that the particles are equally coated independent of their initial size. The SEM photograph of particles grown for 180 min is shown in Fig.3. The almost spherical shape of $(3.0 \pm 0.1)\,\mu$m diameter shows that particles have also been coated isotropically.

COULOMB CRYSTAL FORMATION

When carbon particles were kept growing, it began to be seen in video pictures that the liquid pattern freezes in the illuminating laser beam after approximately 30 min. This indicates that particles were fixed and ordered in the plasma-sheath boundary above the lower (grounded) electrode. Interparticle distance was enlarged with time and the arrangement could be seen more clearly. Figures 4(a) and 4(b) show photographs of the ordered particles taken at 180 min after the injection viewed from a side viewport and from an upper viewport through a 3mm diameter hole in the rf electrode, respectively. It can be seen from Fig.4(a) that particles are arranged laterally in five layers, and also in the vertical direction. The arrangement of the particles in the lateral plane seen in Fig.4(b) is closely-packed and identified to be hexagonal, although some disorders or lattice mismatches are observed. Most of the lattice points do not indicate deviation or fuzziness although several layers were stacked vertically. This means that the particles are mostly aligned vertically, and each lattice point consists of one particle. From these observations, it can be concluded that particles formed a Coulomb crystal in the closely packed hexagonal structure as illustrated three dimensionally in Fig.4(c). Thus, it is suggested that lateral force between the particles is isotropic in the plane. However, the force acting in the vertical direction, which includes Coulomb, gravity, electric field, ion drag forces and others, must be compressive overall. The mean interparticle distances are estimated from the photographs to be 290 μm in the lateral direction and 220 μm in the vertical direction, respectively.

The time evolutions of the particle density N, diameter d and the Wigner-Seitz radius $a = [3/(4\pi N)]^{1/3}$ determined by MSE are plotted in Fig.5. Discontinuities in the growth rate of the diameter and the

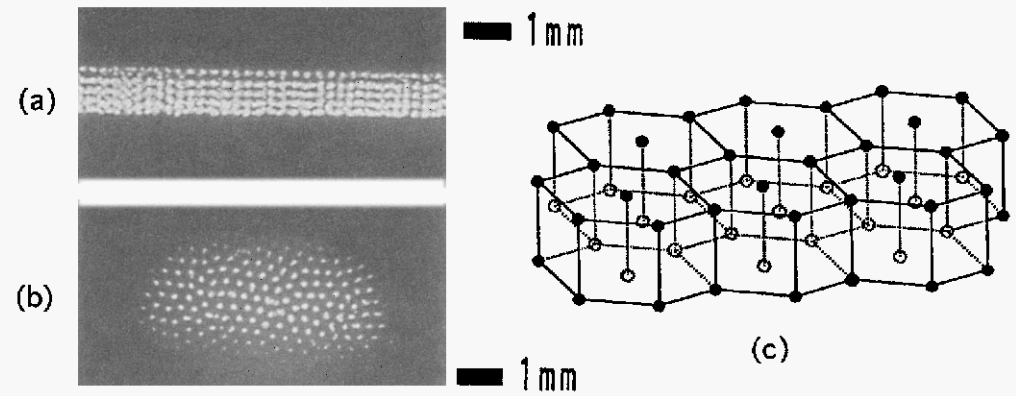

Fig.4 Photographs of the Coulomb solid taken from (a) side viewport and (b) top viewport, and (c) an image of the three-dimensional structure.

Wigner-Seitz radius are seen at 25-30 min. The change occurs when the arrangement starts to be recognized in the photographic or video observation. From this correspondence, it is suggested that Coulomb solidification occurs in that period. The discontinuity in the density or the Wigner-Seitz radius at solidification is considered to occur as follows. Before solidification, the particle density is too high, so that the particles can not attach enough electrons to couple strongly with each other(2), and they escape easily from the plasma region. However, as the density decreases and the particle charge increases, the particles begin to interact mutually via shielded Coulomb potential to form the solidified state by reducing the free energy of the state(11). Then, their loss is suppressed and the density is kept almost constant. The growth rate of particles is constant at 50nm/min before the solidification. It slows down to 19 nm/min just after the solidification, and then to 5 nm min at 180 min, although it is still much larger than the film deposition rate on the grounded electrode of 0.9 nm/min.. From the discontinuity in the particle growth rate, it appears that the growth mechanism changes after the solidification. Although details have not yet been clarified for the early fast growth rate, it might be related to mutual coalescence and ion reactions, as has been argued for particle growth in silane plasma(12,13). The slower growth after the solidification can be attributed to deposition only by neutral radicals. The transport of neutral radicals to particles in plasma is governed by the free flux due to their thermal motion in contrast to the diffusional transport to the electrode.

The negative charge -Q (Q>0) on each particle was evaluated from the particle diameter d and particle density N by the equation

$$1 + \frac{1}{2\pi\varepsilon_0 d}\frac{eQ}{k_B T_i} = \left(\frac{m_i T_e}{m_e T_i}\right)^{1/2}\frac{n_e}{n_i}\exp\left(-\frac{1}{2\pi\varepsilon_0 d}\frac{eQ}{k_B T_e}\right), \qquad (2)$$

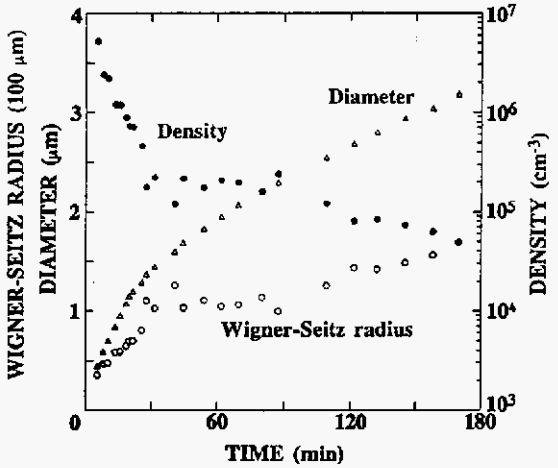

Fig.5 Temporal variations of density, mean diameter and Wigner-Seitz radius of particles obtained by MSE.

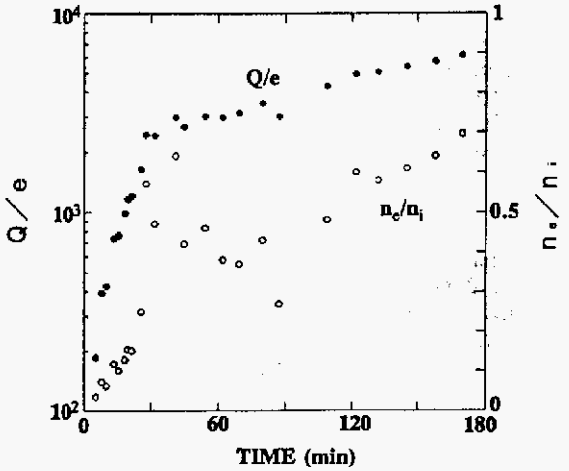

Fig.6 Estimated time variations of the particle charge Q and the ratio of electron density ne to ion density ni.

where m_e is the electron mass, m_i the ion mass, T_e the electron temperature, T_i the ion temperature, n_e the electron density and n_i the ion density. The densities of charged particles are related by the relation for charge neutrality as $n_e + (Q/e)N = N_i$. Equation (2) is based on the balance between the electron current and the ion current flowing into particles derived from the orbital-motion-limited probe theory (14) with $n_e \neq n_i$, under the assumption of a non drifting Maxwellian velocity distribution for electrons and ions.

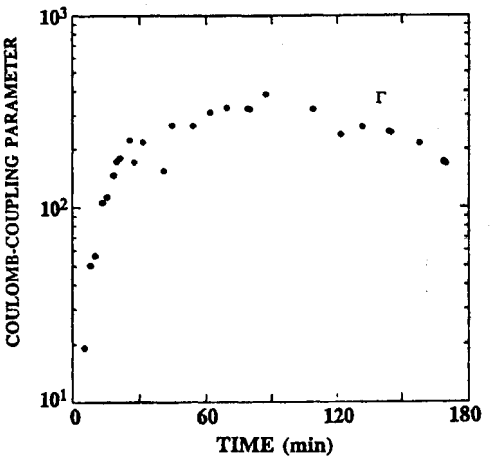

Fig.7 Estimated time variation of the Coulomb-coupling parameter Γ.

Values of Q and n_e were calculated from these equations with the assumed values of 10^9 cm^{-3} for the ion density, 3 eV for the electron temperature and 0.03 eV for the ion temperature, which were estimated from values measured previously under similar conditions in a methane plasma (15). The results are shown in Fig.6. It is seen that n_e/n_i increases before the solidification, abruptly increases at the transition, and then becomes almost constant at about 0.5. It is also seen that Q increases rapidly before the solidification, but then only slowly after the change. These facts suggest the following. Almost all electrons are attached onto particles and negative charge in the plasma is beard mainly by particles before the solidification because the particle density is too high. With a decrease in particle density, Q and n_e/n_i increase. An abrupt increase in n_e/n_i at the solidification is caused by an abrupt decrease in the particle density, which occurs because the particle distribution in the plasma may be rearranged with the change in the Coulomb interaction between particles. After the solidification, bound particles rarely escape from the plasma region, so Q and n_e/n_i change only slowly.

The Coulomb-coupling parameter Γ is defined as the ratio of Coulomb potential energy of particles to thermal kinetic energy as (2)

$$\Gamma = \frac{Q^2}{4\pi\varepsilon_0} \exp\left(-\frac{a}{\lambda_D}\right)/k_B T , \qquad (3)$$

where a is the Wigner-Seitz radius defined before, λ_D is the Debye length, calculated to be 40 μm from the ion density and the ion temperature given above, and T is the particle temperature. Fig. 7 shows the variation of Γ calculated from the data of Fig. 6 under the assumption $T = T_i$. As shown, Γ increases rapidly at first, reaching about 200 at the time of solidification, and then changes slowly. The Γ value of 200 for the liquid-to-solid phase transition is close to the value of around 170 calculated by a Monte Carlo simulation (11). The change in Γ also supports the view that the transition has occurred at 25-30 min. It has been reported that a Coulomb solid can be formed only with monodisperse particles (16). From our experiment, it can be concluded that monodisperse spherical particles have been grown by deposition, and this has helped the formation of a Coulomb solid through a liquid phase in the plasma.

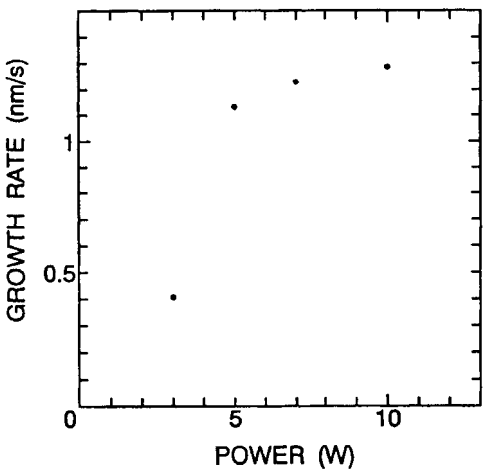

Fig.8 Dependence of the particle growth rate on the rf power at a fixed pressure of 40 Pa.

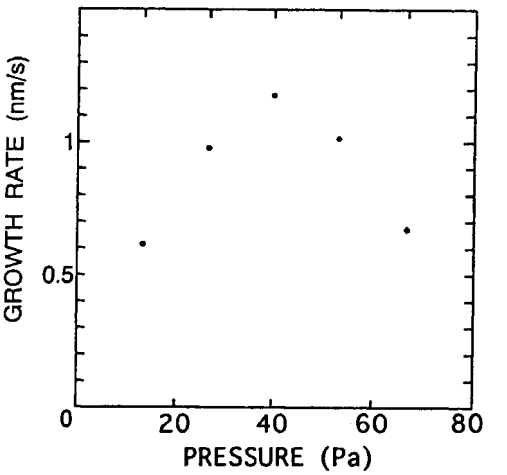

Fig.9 Dependence of the particle growth rate on the gas pressure at a fixed rf power of 5 W.

TOWARD SYNTHESIS OF TAILORED PARTICLES

Under various plasma conditions, particle growth rate before Coulomb crystal formation was evaluated using MSE. The dependence of the growth rate on the rf power at a pressure of 40 Pa is shown in Fig.8. It is seen that the growth rate increases linearly up to 5 W, but then slows down. This means that the coating process goes into the gas supply rate-limiting condition. Under the rf power more than 10 W, particles tended to be concentrated in positions of strong electric field. Fig.9 shows the pressure dependence of the growth rate at a fixed rf power of 5 W. Maximum growth rate was obtained at 40 Pa. It is suggested that the increase in the growth rate with pressure up to 40 Pa is due to the increase in the production rate of depositing precursors. However, at higher pressure the electron energy tends to decrease, and possibly it causes the lowering of the production rate and makes the the growth rate slower.

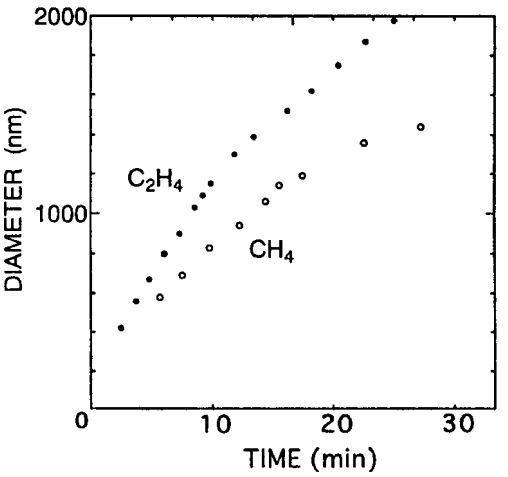

Fig.10 The growth rate of carbon particles with methane and ethylene as source gases.

Instead of methane we tried to supply ethylene as an alternative source gas into the reactor under the same plasma conditions (gas pressure of 40 Pa an rf power power of 5 W). As seen in Fig.10, the growth rate increased by a factor of about 1.7. Thus, it is suggested that in the ethylene plasma main depositing precursor may contain two carbon atoms, if the density is comparable to the precursor in the methane plasma (presumably methyl radical). Otherwise, if the precursor is the same as in the methane plasma, its production rate must be faster by that factor. However, it should be noted that the particle nucleation through polymerization of precursors in the plasma may occur if the supply of precursors is too fast. Actually, with ethylene gas of 40 Pa in this experiment, the generation of particle nuclei was observed when the discharge power became higher than 10 W.

We tried also to put a metal ring (3.5 cm in outer diameter, 3 cm in inner diameter and 0.3 cm in thickness) on the grounded electrode in order to modify the electric field for suppressing the radial loss of particles. Then, it was observed noticeably that he density loss of particles trapped over the inner circle became much smaller after the solidification. Based on the experimental background given above, the synthesis of particles with tailored structures is going to be performed, e.g., by switching the source gases from methane to silane or by coating the particles with vaporized metal.

REFERENCES

(1) J.P. Boeuf, G.S. Selwin and M.J. Kushner ed.,*Proc. NATO Adv. Res. Workshop on the Formation, Transport and Consequences of Particles in Plasmas,* as special issue in *Plasma Sources, Sci. & Technol.* **3**(3), (1994).
(2) H. Ikezi, *Phys. Fluids* , **29**, 1764 (1986).
(3) Y. Hayashi and K.Tachibana, *Jpn. J. Appl. Phys.* **33**, L804 (1994).
(4) J.H. Chu and Lin I, *Phys. Rev. Lett.* . **72**, 4009 (1994).
(5) H. Thomas, G.E. Morfill, V. Demmel, J. Goree, B. Feuerbacher, and D. Mohlmann, *Phys. Rev. Lett.* **73**, 652 (1994).
(6) Y.Hayashi and K.Tachibana, *Jpn. J. Appl. Phys.* **33**, L476 (1994).
(7) Y.Hayashi and K.Tachibana, *Jpn. J. Appl. Phys.* **33**, 4208 (1994).
(8) H.C. van de Hulst, *LIght Scattering by Small Particles* p.125, Dover, New York (1981).
(9) D. Deirmendjian, *Electromagnetic Scattering on Spherical Polydispersions* , p.71, American Elsevier, New York (1969).
(10) Y. Hayashi, *Jpn. J. Appl. Phys.* 29, 2514 (1990).
(11) W.L. Slattery, G.D. Doolen, and H.E. DeWitt, *Phys. Rev. A* , **21**, 21 (1980).
(12) Y. Watanabe and M. Shiratani, *Jpn. J. Appl. Phys.* **32**, 3074 (1993).
(13) J. Perrin, *Plasma Sources Sci. Technol.*. **3**, 252 (1994).
(14) L. Shott, in *Plasma Daignostics*, ed. W. Lochte-Holtgreven (Wiley, New York, 1970) chap.11.
(15) T. Tatsuta, T. Okuno, K. Tachibana, and O. Tsuji, *Proc. 8th Symp. on Plasma Processing* , p.77, Div. Plasma Electronics in Jpn. Soc. Appl. Phys., Tokyo (1991).
(16) R. McRae and A.D.J. Haymet, *J. Chem. Phys.* **88**, 1114 (1988).